Dissertations, Master's Theses and Master's Reports - Open

Dissertations, Master's Theses and Master's Reports

2014

THE THREE DIMENSIONAL SHAPE AND ROUGHNESS OF MINERAL DUST

Xinxin Woodward
Michigan Technological University

THE THREE DIMENSIONAL SHAPE AND ROUGHNESS

OF MINERAL DUST

By

Xinxin Woodward

A REPORT

Submitted in partial fulfillment of the requirements for the degree of

MASTER OF SCIENCE

In Physics

MICHIGAN TECHNOLOGICAL UNIVERSITY

2014

This report has been approved in partial fulfillment of the requirements for the Degree of MASTER OF SCIENCE in Physics.

Department of Physics

Report Advisor: *Dr. Will Cantrell*

Committee Member: *Dr. John A Jaszczak*

Committee Member: *Dr. Alexander B. Kostinski*

Committee Member: *Dr. Louisa J. Kramer*

Department Chair: *Dr. Ravindra Pandy*

Table of Contents

Acknowledgements

I specially thank for Dr. Cantrell for his guidance and full support. He encourages me and raises my confidence. Dr. Canrell is always very patient when he's helping me, even with small bug in matlab programing to lots of grammar and English in posters, papers and reports.

I would also like to thank Dr. Alex Kostinski for his guidance and he raised some brilliant ideas for expressing roughness.

Dr. John Jaszczak was longing us AFM and offered lots of help on getting started, we really appreciated that.

I also want to thank Swarup China for work collaborating with us and sharing SEM data.

I would like to thank the Michigan Tech Department of Physics for providing the tools necessary for success.

Finally, I would like to express my gratitude to the NSF for the funding and support to our work.

Abstract

Mineral dust shape and roughness are important for a multitude of processes; it is known for aspherical shape but the true measurements in three dimensions are rare. Atomic Force Microscope was used for determine both 3D shape and roughness for two dust which are commonly used in laboratory experiments – Arizona Test Dust (ATD) and Kaolinite. We determined both of them are rather flat and round; an oblate spheroid would be a good model. Loess Filter was used to smooth the particles' surface and correlation analysis was used to examine the surfaces' properties of the dust; we found no features under 100nm scales. Also, our particles' surface area result is very similar to BET surface area.

1. Introduction

Mineral dust is the most abundant class of aerosol particle in atmosphere by mass (Cakmur et al., 2006). Dust particles also play an important role in the atmosphere. They scatter and absorb solar and terrestrial radiation, catalyze cloud formation at low supersaturations (cloud condensation nuclei) (Van den Heever et al., 2006). They also can initiate freezing below water's melting point as ice nuclei (Hoose and Möhler, 2012). Roughly 50% of individual cloud ice residual is mineral dust (Pratt et al., 2009). For the open ocean, dust is also an important nutrient (Schulz et al., 2012; Formenti et al., 2011).

The lifetime being air born of dust governs the dust influence to Earth's atmosphere. For instance, large particles tend to have shorter lifetimes in the atmosphere. They settle out close to the region where they were emitted. In comparison, small particles have longer lifetimes to travel much further, even across oceans (Liu et al., 2013). Both shape and roughness of particles are important for determine a particles' lifetime in atmosphere; particles have a larger surface area to mass ratio (e.g. small particle or particle with rough surface) would have a greater drag force that would reduce falling speed, therefore extending their lifetime in the atmosphere(Yang et al., 2011).

Mineral dust is important for ice nuclei (IN); some types of mineral dust are better ice nuclei than others (Meland et al., 2012). With the limited understanding we have for ice, we think the shape, roughness, composition, and net charge or electric field at the particle surface are the main reasons for the variation of ice nucleation in clouds. (Ehre et al., 2010; Okada et al., 2001).

Even though shape is an important factor for all the reasons above, Formenti et al. (2011) mentioned "data on the third dimension of particles and the surface roughness are very rare but are needed for optical modeling". There have been many studies which just assumed particles are spherical for modeling; furthermore, the most common device for reporting size distribution, the Scanning Mobility Particle Sizer (SMPS), also assumes the particles are spherical and only output the mobility diameter distribution.

There have been studies of shape characteristics about dust particles. Both Scanning Electron Microscopy (SEM) and Atomic Force Microscopy (AFM) are good tools to analyze dust particles

(Vijendran, 2007). SEM scans the sample surface by shooting an electron beam at it and receiving a signal back from atoms on the surface. SEM gives a very detailed picture but it is not well suited to measure for the particles' heights (Reid et al., 2003), because the brightness in the SEM image is related to the composition of the sample and its curvature. Okada et al. (2001) coated particles with a Pt/Pd alloy at an angle of 26.6 degrees and calculated the height of the particle by measuring the shadow. They found out that the mean height of the particles is only 5 to 10% of the maximum length. People started noticing that the optical properties of mineral clay aerosol can be assumed as highly eccentric oblate spheroids (Meland et al., 2012).

Instead of electron beams shooting to the surface, AFM uses a probe with sharp tip on a cantilever moving across the surface of the sample row by row. While going through a non flat area, the tip would shift up and down. A laser directed on the tip and if the tip shift up and down, the receiver would detect a change in intensity. From there, AFM calculates the surface height for each point the tip detects.

AFM is a natural tool for not only shape properties but also for analyzing surface roughness. Hela and Andreae (2008) found that Sahara dust particles are rather smooth, and Chou et al. (2008) also think particles are smooth. Both papers only mentioned that the dust particles used were smooth, but to what level of smoothness was not explained.

This work uses the AFM to image two types of mineral dust: Arizona Test Dust (ATD) and Kaolinite. ATD and Kaolinte are well used in laboratory. Even with similar components, ATD is a much better ice nuclei than Kaolinite. We studied the shape properties and expressed their roughness in a few ways; we also compared the two type of dust to see a trend for being better/worse ice nuclei.

2. Method:

2.1. Properties of AFM

We used a Nanosurf Easyscan2 AFM (Nanoscience Instruments) to image mineral dust. To get the best quality images, both contact and dynamic modes were explored for the experiment; the dynamic mode appears to produce much more successful images with reasonable particles because probe tip interacts with sample surface in vertical motion and has a lower chance to shift particles. Contrarily, contact mode 'drags' the probe tip over the entire surface. Cantilever T-190R-10 was used for the dynamic mode; it has a spring contact of 48 N/m and a resonant frequency 190 KHz. We set the probe tip sampling to 2048 times per line for 2048 lines for sample area up to 625μm^2 with lateral resolution 5-25nm and vertical resolution 0.37nm.

2.2 Sample

We would like to use a substrate that is smooth as possible to differentiate and identify the difference of height between the substrate and the mineral dust particle accurately. Mica (Tarheel Mica Co.) is the flattest substrate found and is very easy to use – simply use pointy tools to poke sideways into the layers, then use the tool as a lever to separate mica into two pieces. In this way two fresh surfaces are acquired.

To make sure the particles are stable on mica, there are a few ways to prepare a sample; one was mixing mineral dust in water and using a syringe to deposit it on freshly peeled mica; it takes half an hour for the water to evaporate and at that point the sample is ready to use. We expect when mineral dust is mixed in water, the soluble component of the particle would dissolve into the water; after the water evaporates, the particles are partially cemented onto mica. The other way to prepare a sample is to coat the mica with a sheet of Superglue, then apply dust particles from air on the wet Superglue. After a couple days of drying at room temperature, the sample is ready to use. From the results, there is no difference in shape and roughness by preparation sample in the two ways above.

Table below shows the composition of ATD and Kaolinite. The order of composition is also the order of composition percentage in dust.

Table 1. Compositions of ATD and Kaolinite

ATD	Kaolinite
SiO_2	SiO_2
Al_2O_3	Fe_2O_3
Fe_2O_3	Al_2O_3
Na_2O	MnO
CaO	CaO
MgO	MgO
TiO_2	H_2O
K_2O	--

From the table we can see the top three compositions which take the most important role are the same, we can conclude the components are similar.

2.3 Shape analysis

After mineral dust particle images were acquired by AFM, we identified and isolated particles with Nanoscience easy scan2 software. Once we had each individual particle image, we exported it into a square matrix with each number representing the height of that point; each neighboring row and column is a resolution apart physically. With the matrices, further analysis was developed with MatLab.

The figure below shows the 3D images of ATD and Kaolinite.

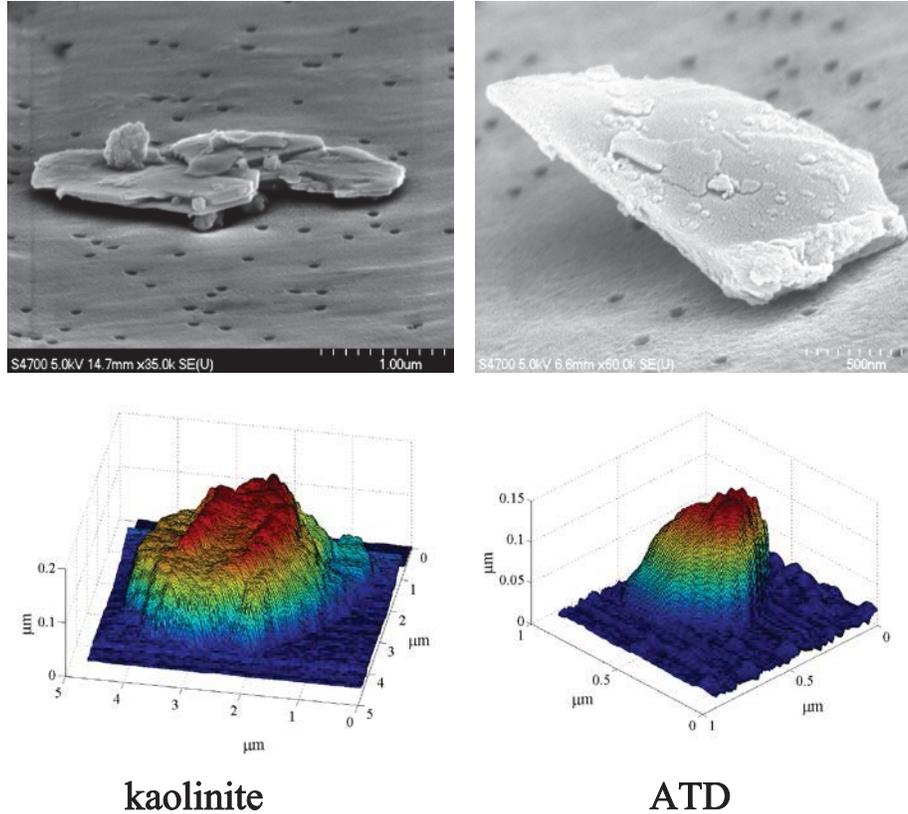kaolinite   ATD

Figure 1. The top row are SEM images, the bottom row are AFM images plotted by MatLab. Note: all images are different particles; it's not possible to image the same particle for both SEM and AFM. The SEM images were taken with tilted sample stage. The height and lateral scale are different for AFM images.

The first step in the analysis was to level background and zero the background noise. After that, we drew out the base contour. With that done, some shape properties were measured, defined, and calculated.

Max length (L_{max}) is the longest distance between two points on the contour; max height (H_{max}) is the highest point of the particle; projected area, A_p, is the area inside contour; area equivalent diameter (D_{aeq}), is the diameter of a circle which has the same amount of area as the contour area.

$$D_{aeq} = \sqrt{\frac{4A_p}{\pi}} \tag{1}$$

The area of the surface which can be detected by AFM (S_m) was calculated with Heron's formula with the vertices (h_i for the ith point) and lateral resolution (r). Since the bottom of the

particle cannot be detected by AFM, we take projected area into account, so the surface area of the particle (S) reported here is

$$S = S_m + A_p \tag{2}$$

The uncertainty and the calculated to 'true value' percentage are mentioned in conclusion and discussion.

For volume of the particles, we assumed each point is a cuboid with two sides being resolution size and the third side being vertex size. So the volume can be expressed as

$$V = \sum r^2 \times h_i \tag{3}$$

2.4 Roughness analysis

From figure 2 you can see there is certain level of roughness on the flat surface from both SEM and AFM image. People have a hard time defining the general shape for each type of particle; also, the same feature might be identified to be both roughness and shape depending on the different scale used. There is not yet a standardized method for analyzing particle roughness.

We represented roughness of particles in a couple of ways. They all require numerically smoothing the particle, and then we compared the smoothed particle with the original one.

We used a loess filter for smoothing; it uses local weighted linear regression to smooth our particle row by row and column by column. The smoothed particle shape depends on the window size; with a small window, the smoothed particle looks rather like the original one; on the other hand, a particle smoothed with a large window looks as if more of the smaller features have been 'washed off'.

Figure 2 shows a cross section of a particle with original vertices, smoothed vertices and residues.
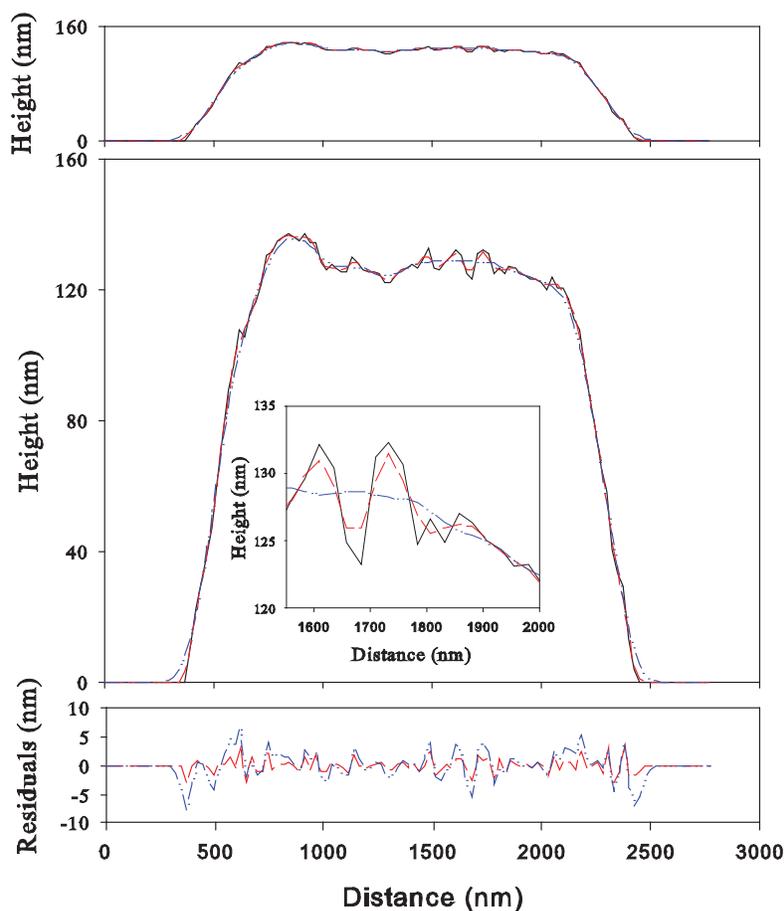
Figure 2. all image shows information from the same cross section. The top image shows the actual height to lateral ratio. The middle image shows a detailed difference between original data (black line), smoothed by 5 point window data (red dash line) and smoothed by 11 point window data (blue dash line). The bottom image shows the difference between both smoothed by 5 point widow data (red dash line) and smoothed by 11 point window data (blue dash line). Be aware that the larger smoothing window creates a bigger residual.

As a first measure of particle roughness, we calculated both the smoothed particles (in different smoothing window) surface area and the original surface area, and then we compared them to see how different they are.

In the next step we subtracted the original from smoothed particle matrix to produce residuals. We lined up all residuals row by row and formed one series. We used a combination of smoothing windows in the loess filter and correlation analysis to detect feature sizes on the particles' surface.

2.5 SEM measurement

Aerosol particles analyzed via Scanning Electron Microscopy were dispersed with a fluidized bed (TSI, 3400A), then collected on 13 mm diameter Nuclepore clear polycarbonate filters with a pore size of 0.1μm (Whatman Inc, Chicago, Illinois, USA) mounted in Costar Pop-Top membrane holders. The sample flow was split before the membrane filter and the second line was connected to a condensation particle counter (CPC, TSI 3772) to monitor the aerosol concentration. After the particles had been collected, the filters were mounted to aluminum stubs and coated with a 1.6nm Pt/Pd alloy layer using a Sputter coater (Hummer™ 6.2) for scanning electron microscopy analysis. The coated filters were imaged using an Hitachi S-4700 field emission scanning electron microscope.

SEM micrographs of dust particles were processed using the freely available ImageJ software (National Institute of Health). High magnification images of dust particles were used to estimate morphological parameters. Each particle was individually processed and threshold were adjusted to convert the image into a binary image the parameters calculated from the binary images were the maximum projected image, and the total projected area of the particle, A_p.

3. Result and Discussion:

3.1 shape

From both SEM and AFM, we see the top down view of particles and noticed that most particles are rather round. We compared the max length of contour and the area equivalent diameter.

Figure 3 shows the ratio $\frac{D_{aeq}}{L_{max}} = 0.7 \pm 0.1$ for both ATD and Kaolinite from the SEM data.
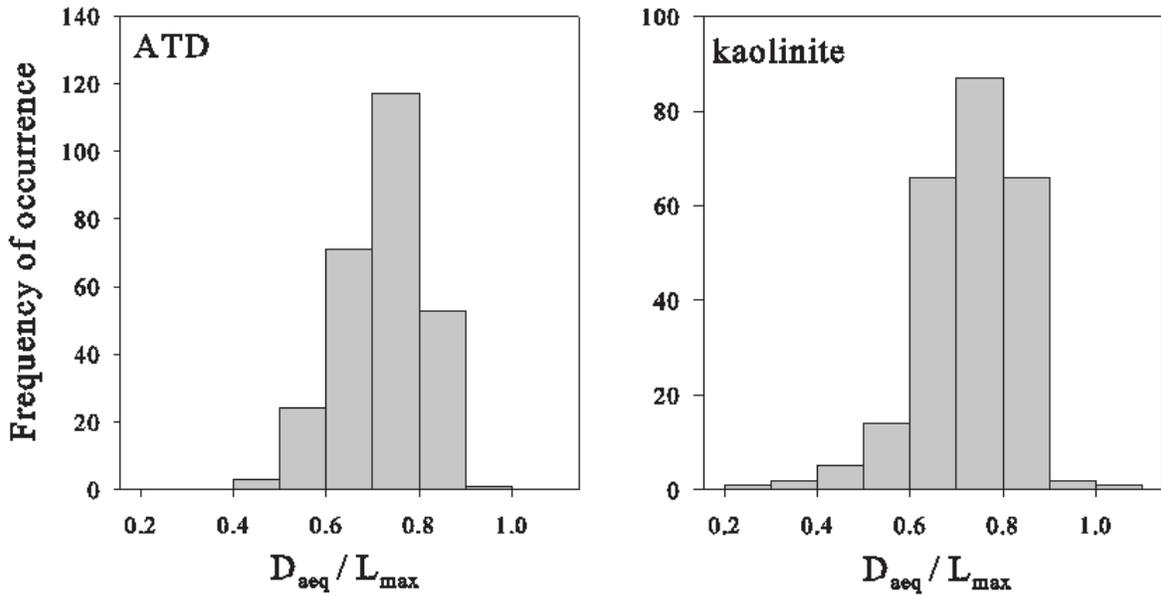
Figure 3. Histogram plots of D_{aeq}/L_{max} by SEM detected particles.

AFM shows a similar result; for ATD, $\frac{D_{aeq}}{L_{max}} = 0.8 \pm 0.1$ and for Kaolinite, $\frac{D_{aeq}}{L_{max}} = 0.76 \pm 0.08$.

While collecting and analyzing data with AFM, we noticed that the height is an order of magnitude smaller than the max length. Figure 4 shows the H_{max} vs. D_{aeq}.
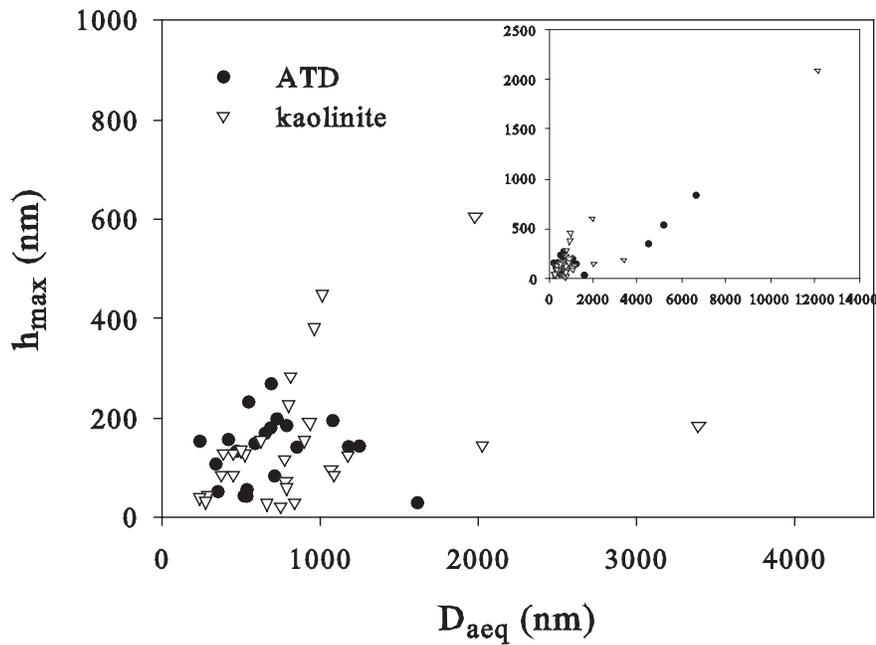

Figure 4. The max height vs. area equivalent diameter by AFM data

The max height is also an order of magnitude smaller than the Area equivalent Diameter. With the conclusion above, we think instead of spherical shape that has been used to model dust, an oblate spheroid would be a better choice.

3.2 Surface area

3.2.1 Surface area analysis

With the surface area we calculated, we can calculate area per mass by using density 2.65 g/cm^3 for ATD and 2.6 g/cm^3 for Kaolinite. We found ATD area per mass is $4.4\ m^2/g$ and Kaolinte is 10.2 m^2/g. The BET surface area for ATD is 5.7 m^2/g (Wagner et al.), which is 77% of our value; The BET surface area for Kaolinite is in the range of 8 to 20 m^2/g depends on the source of the kaolinite (Bickmore et al. 2002); our result falls in to the range.

3.2.2 Surface uncertainty analysis

Since the AFM can't detect the particle area facing the substrate, there is uncertainty in our area calculation. With the result from 3.1, we can assume our particles are oblate spheroids; we found uncertainty by computing an oblate spheroid model, assuming there is AFM detecting over the oblate spheroid and result a matrix of vertices with the center point of the matrix being the highest point in oblate spheroid.

Figure below shows a 3D oblate spheroid particle 'detected' by AFM that we constructed.
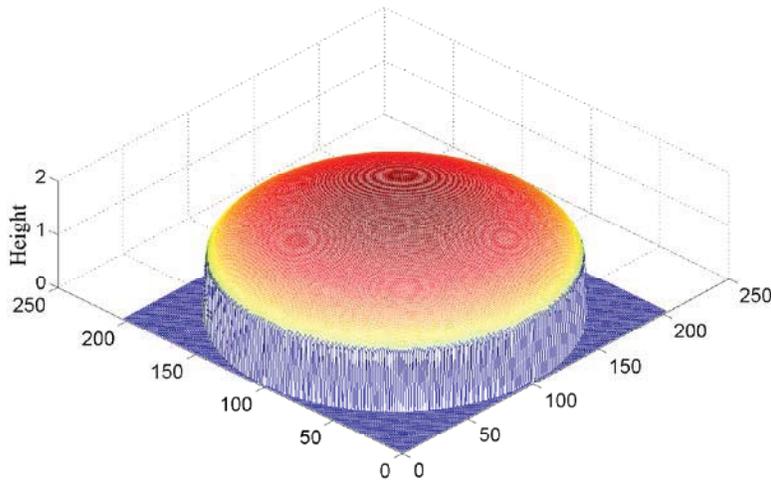
Figure 5. we set oblate spheroid major axis R= 10, resolution of AFM 0.1, and the aspect ratio (major axis / minor axis) is 10 which results in a ΔS of 10%

After set up the matrix, we calculate the surface area just like a real particle and find the difference in ratio by

$$\Delta S = \frac{S_{oblate} - S_{model}}{S_{oblate}} \tag{4}$$

Where S_{oblate} is the oblate spheroid surface area and S_{model} is the model's surface area.

In the model, with a bigger $major\ axis/resolution$ ratio, we would have smaller percentage difference; which leads to a smaller uncertainty, and with a higher aspect ratio, the particle is closer to the ground, which also reduces the uncertainty. For ATD, the average aspect ratio is 8 and the average D_{aeq}/r ratio is 130, which result 12% difference; For Kaolinite, the average aspect ratio is 9 and the average D_{aeq}/r ratio is 103, which result in an 11% difference.

From the information above, if the particle is oblate spheroid like shape, the uncertainty would be in the range of 8~15% of the actual value above the actual value.

3.3 Roughness

3.3.1 Surface area difference

With the roughness analysis method, we first smoothed the original particle over and over again with the same window size, and then we smoothed the original particle with different window size, from 5 points per window up to 13 points per window. Next, we calculated surface area for all of the smoothed particles, and divided them by the original surface area (S/S_0). Figure 6 shows the ratios for both ATD and Kaolinite.
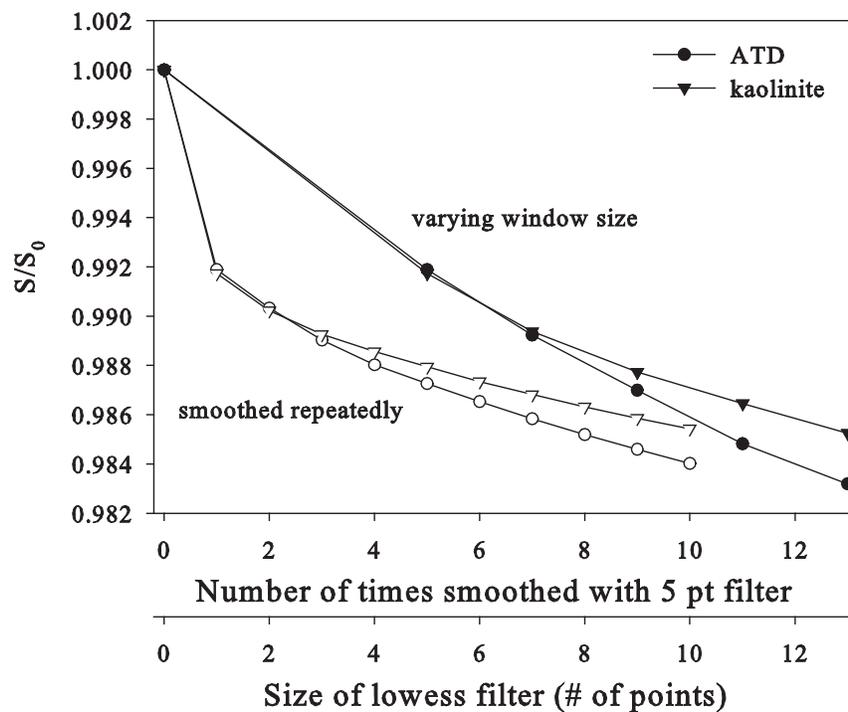

Figure 6. ATD and Kaolinite S/S_0 for both number of times smoothed with 5 point window (hollowed circle and triangle) and 5 to 13 window size (filled circle and triangle) by AFM data

The first evidence is that the surface area decreased as the number of time smoothed increase and also as the window size increased, which is also as expected.

We also found out that none of the smoothed particle is more than 2% smaller than original particle, which indicates there aren't obvious features under 13 points window size, which is in the average of 130nm. However, we can't smooth particles with a larger window because the outline of the particle might be evolved as well.

12

3.3.2 Autocorrelation analysis

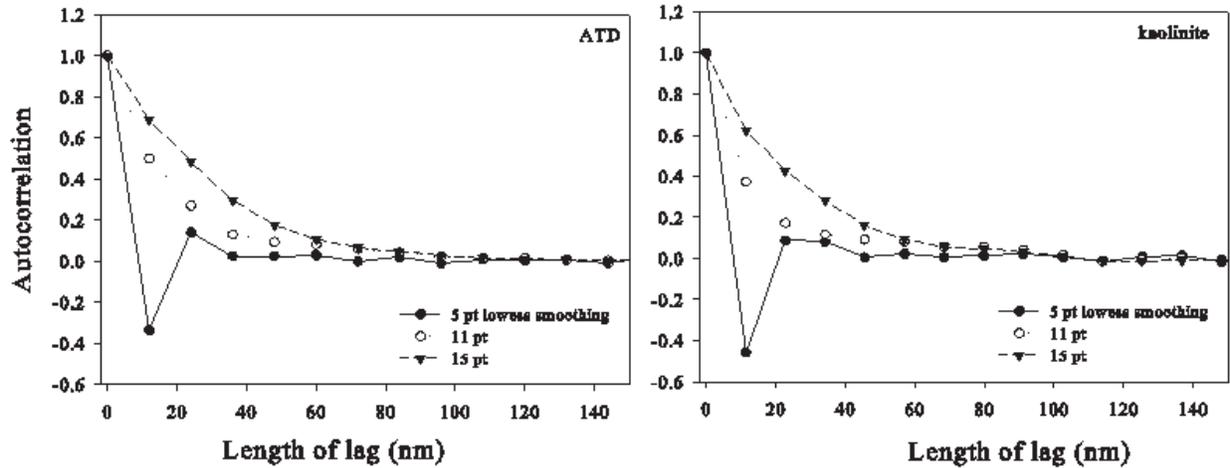The figure below shows the correlation as a function of length of lag.

Figure 7. Autocorrelation function with varied length of lag by AFM data

Both ATD and Kaolinite shows with 5 points window loess smoothing, the correlation decays to zero; it suggested that there are not many measureable features in that scale (around 50nm in average). With the other correlations by residual from 11 points and 13 points window decays much more slowly. Which means there are features above 100nm in size; or we could say the roughness is in 100nm scale or above.

Even though the data we collect from AFM is around 10 nm resolution on average, which is 100 Å, we can't receive the roughness under that resolution level, but since the BET number mentioned above and our calculation are substantially the same; we conclude that in atomic level, the ATD and Kaolinite are not very rough.

4. Summary

Arizona Test Dust and Kaolinite are round and flat, oblate spheroid like. They don't have a manifest shape difference and their horizontal to height scale are both eight on average.

Also, both types of particles are smooth, we expect no feature below 100nm scale. This model can be used for radiative transfer, transport, and chemical reactions upon the dust.

5. Reference:

Bickmore, B. R., Nagy, K. L., Sandlin, P. E., Crater, T. S., May 2002. Quantifying surface areas of clays by atomic force microscopy. American Mineralogist 87(5-6), 780-783

Cakemur, R. V., Miller, R. L. Perlwitz, J., Geogdzhayev, I. V., Ginoux, P., Koch, D., Kohfeld, K. E., Tegen, I., Zender, C. S., 2006. Constraining the magnitude of the global dust cycle by minimizing the difference between a model and observations. Journal of Geiphysical Research: Atmospheres 111(D6), n/an/a

Chou, C., P. Formenti, M. Maille, P. Ausset, G. Helas, M. Harrison, and S. Osborne (2008), Size distribution, shape, and composition of mineral dust aerosols collected during the African Monsoon Multidisciplinary Analysis Special Observation Period 0: Dust and Biomass-Burning Experiment field campaign in Niger, January 2006, J. Geophys. Res., 113, D00C10, doi: 10.1029/2008JD009897.

Ehre, D., et al. (2010). "Water Freezes Differently on Positively and Negatively Charged Surfaces of Pyroelectric Materials." Science 327(5966): 672-675.

Formenti, P., Schütz, L., Balkanski, Y., Desboeufs, K., Ebert, M., Kandler, K., Petzold, A., Scheuvens, D., Weinbruch, S., and Zhang, D.: Recent progress in understanding physical and chemical properties of African and Asian mineral dust, Atmos. Chem. Phys., 11, 8231-8256, doi:10.5194/acp-11-8231-2011, 2011.

Helas, G. and Andreae, M. O.: Surface features on Sahara soil dust particles made visible by atomic force microscope (AFM) phase images, Atmos. Meas. Tech. Discuss., 1, 1-19, doi:10.5194/amtd-1-1-2008, 2008.

Hoose, C. and Möhler, O.: Heterogeneous ice nucleation on atmospheric aerosols: a review of results from laboratory experiments, Atmos. Chem. Phys., 12, 9817-9854, doi:10.5194/acp-12-9817-2012, 2012.

Zhaoyan Liu, T. Duncan Fairlie, Itsushi Uno, Jingfeng Huang, Dong Wu, Ali Omar, Jayanta Kar, Mark Vaughan, Raymond Rogers, David Winker, Charles Trepte, Yongxiang Hu, Wenbo Sun, Bing Lin, Anning Cheng, Transpacific transport and evolution of the optical properties of Asian dust, Journal of Quantitative Spectroscopy and Radiative Transfer, Volume 116, February 2013, Pages 24-33, ISSN 0022-4073, http://dx.doi.org/10.1016/j.jqsrt.2012.11.011.

B. Meland, J.M. Alexander, C.-S. Wong, V.H. Grassian, M.A. Young, P.D. Kleiber, Evidence for particle size–shape correlations in the optical properties of silicate clay aerosol, Journal of Quantitative Spectroscopy and Radiative Transfer, Volume 113, Issue 7, May 2012, Pages 549-558, ISSN 0022-4073, http://dx.doi.org/10.1016/j.jqsrt.2012.01.012. (http://www.sciencedirect.com/science/article/pii/S0022407312000283)

Okada, K., Heintzenberg, J., K., Qin, Y., 2001. Shape of atmospheric mineral particles collected in three Chinese arid-regions. Geophys. Res. Lett. 28(16), 31233126

Kerri A. Pratt, Paul J. DeMott, Jeffrey R. French, Zhien Wang, Douglas L. Westphal, Andrew J. Heymsfield, Cynthia H. Twohy, Anthony J. Prenni2 & Kimberly A. Prather (2009). "In situ detection of biological particles in cloud ice-crystals." Nature Geosci 2(6): 398-401.

Reid, E. A., J. S. Reid, M. M. Meier, M. R. Dunlap, S. S. Cliff, A. Broumas, K. Perry, and H. Maring(2003), Characterization of African dust transported to Puerto Rico by individual particle and size segregated bulk analysis, J. Geophys. Res., 108, 8591, doi:10.1029/2002JD002935, D19.

Schulz, M., Prospero, J. M., Baker, A. R.,Dentener, F., ickes, L., Liss, P. S., Mahowald, N. M., Nickovic, S., Garcia-Pando, C. P., Rodriguez, S., Sarin, M., Tegen, I., Duce, R. A., Oct. 2012. Atmospheric transport and deposition of mineral dust to the ocean: Implications for research needs. Environ. Sci. Technol. 46(19), 10390-10404.

Van den Heever, Susan C., Gustavo G. Carrió, William R. Cotton, Paul J. DeMott, Anthony J. Prenni, 2006: Impacts of Nucleating Aerosol on Florida Storms. Part I: Mesoscale Simulations. J. Atmos. Sci., 63, 1752–1775.   doi: http://dx.doi.org/10.1175/JAS3713.1

VIJENDRAN, S., SYKULSKA, H. and PIKE, W. T. (2007), AFM investigation of Martian soil simulants on micromachined Si substrates. Journal of Microscopy, 227: 236–245. doi: 10.1111/j.1365-2818.2007.01806.x

Wagner, C., F. Hanisch, N. Holmes, H. de Coninck, G. Schuster, and J. N. Crowley. "The interaction of N2O5 with mineral dust: aerosol flow tube and Knudsen reactor studies, Atmos. 30 Chem. Phys., 8, 91–109, 2008.

Yang, W., A. Marshak, A. B. Kostinski, and T. Várnai (2013), Shape-induced gravitational sorting of Saharan dust during transatlantic voyage: Evidence from CALIOP lidar depolarization measurements, Geophys. Res. Lett., 40, 3281–3286, doi:10.1002/grl.50603.